10. S. Carranza, J. Baguñà, M. Riutort, *Mol. Biol. Evol.* **14**, 485 (1997).
11. D. T. J. Littlewood, K. Rohde, K. A. Clough, *Biol. J. Linn. Soc.* **66**, 75 (1999).
12. J. Felsenstein, *Syst. Zool.* **27**, 401 (1978); G. J. Olsen, *Cold Spring Harb. Symp. Quant. Biol.* **LII**, 825 (1987).
13. The 18*S* rDNA was amplified and sequenced from high molecular weight genomic DNA as described [(*11*); S. Carranza, G. Giribet, C. Ribera, J. Baguñà, M. Riutort, *Mol. Biol. Evol.* **13**, 824 (1996)].
14. Sequences have been deposited in the GenBank under accession numbers AF102892 to AF102900 and AJ012522 to AJ012530.
15. Sequences were aligned by eye on the basis of the secondary structure model [R. R. Gutell, B. Weibser, C. R. Woese, H. F. Noller, *Prog. Nucleic Acid Res. Mol. Biol.* **32**, 155 (1985)] with GDE v.2.2. Positions that could not be unambiguously aligned were removed from the alignment. The final matrix contained 1181 sites (including 584 variable, 383 informative under parsimony); the full final alignment is deposited under accession number ds37667.dat and is available at ftp://FTP.EBI.AC.UK under directory pub/databases/embl/align.
16. The relative rate test [A. C. Wilson, S. S. Carlson, T. J. White, *Annu. Rev. Biochem* **46**, 573 (1977)] compares genetic distances between each of two species and a reference outgroup. We performed the test according to W. H. Li and M. Tanimura, *Nature* **326**, 93 (1987). A first set of 45 bilaterian species (deuterostomes; ecdysozoans, with the exception of Nematoda; and lophotrochozoans, with the exception of Platyhelminthes) with slow and uniform rates of nucleotide substitution, as reflected in their similarly short branch lengths in most published phylogenetic trees, were selected and compared by pairs with diploblasts as reference outgroups. As expected, all were found to have uniform relative rates of nucleotide substitution. Then, a second set of 29 bilaterian species from phyla known to have rates higher than the first set (Platyhelminthes including acoels, Nematoda, Chaetognata, Mesozoa, Gnathostomulida, Rotifera, and Acanthocephala) were compared with each of the species of the first group (45 species) with diploblasts as reference. The results are expressed in Table 1 as the number of cases in which each species has a rate significantly different from those of the first group at the 1% and at the 5% levels.
17. H. Philippe, *Nucleic Acid Res.* **21**, 5264 (1993). The analysis shows the relation between the number of changes that have occurred (as deduced from the tree), and the number of changes that can be calculated directly from the sequence alignment. When the sequences are saturated, it is expected that although the number of inferred changes still increases (*x* axis), they are no longer detected as observed differences (leveling along the *y* axis), so the line defined by the points levels off from the diagonal in the graph and becomes horizontal.
18. The likelihood mapping analysis [(*38*); K. Strimmer and A. von Haeseler, *Proc. Natl. Acad. Sci. U.S.A.* **94**, 6815 (1997)] is a graphical method to visualize the phylogenetic content of a set of aligned sequences. Likelihoods of all quartet trees for each subset of four species are mapped on a triangle, and the triangle is partitioned in different regions. The central region represents starlike evolution, the three corners represent well-resolved phylogeny, and three intermediate regions between corners represent where it is difficult to distinguish between two of the three trees. The resulting distribution of points indicates whether or not the data are suitable for a phylogenetic reconstruction: the phylogenetic information in the data is higher when the value in the central region is smaller.
19. Tree reconstruction was performed by maximum likelihood with both fastDNAml v.1.1.1.a [G. J. Olsen, H. Matsuda, R. Hangstrom, R. Overbeek, *Comput. Appl. Biosci.* **10**, 41 (1994)] and PUZZLE v. 4.0 (*38*) programs. We built an initial tree with fastDNAML using global rearrangements and jumble options and subjected it to the Kishino-Hasegawa test against alternative topologies using PUZZLE [HKY model of substitution; M. Hasegawa, H. Kishino, K. Yano, *J. Mol. Evol.* **22**, 160 (1985)]. The parameters for rate heterogeneity among sites were inferred from the data set. The best tree found was resubmitted to a global rearrangement search with fastDNAML, taking into account among-site rate variation by using the rate and category parameters calculated by PUZZLE.
20. T. G. Karling, in *Biology of the Turbellaria*, N. W. Riser and M. P. Morse, Eds. (McGraw-Hill, New York, 1974), pp. 1–16.
21. P. Ax, *The Phylogenetic System. The Systematization of Organisms on the Basis of Their Phylogenesis* (Wiley, Chichester, UK, 1987).
22. U. Ehlers, *Das Phylogenetische System der Plathelminthes* (Fischer, Stuttgart, 1985).
23. J. P. S. Smith, S. Tyler, R. M. Rieger, *Hydrobiologia* **132**, 13 (1986).
24. P. Ax, *Multicellular Animals, A New Approach to the Phylogenetic Order in Nature* (Springer-Verlag, Berlin, 1996).
25. To analyze the support for internal branches in a tree without having to compute the overall tree, we performed four-cluster likelihood mapping using PUZZLE 4.0 (*38*). Every internal branch in a completely resolved tree defines up to four clusters of sequences. These four clusters can be defined in the data file, and the program will build a quartet tree for each of all possible combinations of four species, always taking one from each group. The result is represented on a triangle (*18*). The distribution of points within this triangle indicates the level of support for the internal branch under analysis.
26. We used PUZZLE 4.0 (*38*) to find the parameters for among-site rate heterogeneity. Resulting data were divided into eight categories, each with an assigned rate value (from constant to diverse values of variability). In two successive analyses we eliminated from the 61 species alignment those positions that were more variable (category 8) and also the sites with the two most variable categories (7 and 8). From these new data sets trees were reconstructed with fastDNAML (*19*).
27. An alignment including only the 18 acoel sequences was used to find their most variable positions and those sites [category 8, see (*26*)] were removed from the 61 species alignment. From this new data set trees were reconstructed with fastDNAML (*19*).
28. R. M. Rieger, S. Tyler, J. P. S. Smith, G. E. Rieger, in *Microscopic Anatomy of Invertebrates*, vol. 3, *Platyhelminthes and Nemertinea*, F. W. Harrison and B. J. Bogitsh, Eds. (Wiley-Liss, New York, 1991), pp. 7–140.
29. G. Haszprunar, *J. Zool. Syst. Evol. Res.* **34**, 41 (1996).
30. B. C. Boyer and J. Q. Henry, *Am. Zool.* **38**, 621 (1998); J. J. Henry, M. Q. Martindale, B. C. Boyer, personal communication.
31. B. C. Boyer, *J. Exp. Zool.* **176**, 96 (1971).
32. J. W. Valentine, *Proc. Natl. Acad. Sci. U.S.A.* **94**, 8001 (1997).
33. E. Reisinger, *Z. Zool. Syst. Evolutionsforsch.* **10**, 1 (1972).
34. O. I. Raikova, M. Reuter, E. A. Kotikova, M. K. S. Gustafsson, *Zoomorphology* **118**, 69 (1998); M. Reuter, O. I. Raikova, M. K. S. Gustafsson, *Tissue Cell* **30**, 57 (1998).
35. G. A. Wray, J. S. Levinton, L. H. Shapiro, *Science* **274**, 568 (1996); F. J. Ayala, A. Rzhetsky, F. J. Ayala, *Proc. Natl. Acad. Sci. U.S.A.* **95**, 606 (1998); L. Bromham, A. Rambaut, R. Fortey, A. Cooper, D. Penny, *ibid.* **95**, 12386 (1998).
36. G. Jägersten, *Evolution of the Metazoan Life Cycle: A Comprehensive Theory* (Academic Press, London, 1972); R. M. Rieger, *Am. Zool.* **34**, 484 (1994).
37. S. Conway-Morris, *Bioessays* **20**, 676 (1998).
38. K. Strimmer and A. von Haeseler, *Mol. Biol. Evol.* **13**, 964 (1996).
39. We thank M. Martindale, J. Henry, and B. Boyer for their insightful comments and sharing of previous results; S. Carranza for his help in the first stages of this work; A. Adoutte, J. McInerney, G. Olsen, H. Philippe, and K. Strimmer for methodological advice; and R. Bray, L. Colin, M. Dawson, A. Faubel, K. Lundin, L. Martin, O. Raikova, R. Rieger, K. Rohde, J. P. S. Smith, and S. Tyler who provided material for this study. I.R.-T., M.R., and J.B. were supported by CIRIT (Generalitat de Catalunya) grants 1995SGR-00574 and 1997SGR-00057. D.T.J.L. and E.A.H. were funded by a Wellcome Trust Senior Research Fellowship to D.T.J.L. (043965/Z/95/Z). J.B. and D.T.J.L. shared the grant HB1996-0034 from the British-Spanish Joint Research Programme (Acciones Integradas).

18 November 1998; accepted 9 February 1999

Rapid Dendritic Morphogenesis in CA1 Hippocampal Dendrites Induced by Synaptic Activity

M. Maletic-Savatic, R. Malinow, K. Svoboda

Activity shapes the structure of neurons and their circuits. Two-photon imaging of CA1 neurons expressing enhanced green fluorescent protein in developing hippocampal slices from rat brains was used to characterize dendritic morphogenesis in response to synaptic activity. High-frequency focal synaptic stimulation induced a period (longer than 30 minutes) of enhanced growth of small filopodia-like protrusions (typically less than 5 micrometers long). Synaptically evoked growth was long-lasting and localized to dendritic regions close (less than 50 micrometers) to the stimulating electrode and was prevented by blockade of *N*-methyl-D-aspartate receptors. Thus, synaptic activation can produce rapid input-specific changes in dendritic structure. Such persistent structural changes could contribute to the development of neural circuitry.

Coordinated patterns of activity help to organize neural circuits throughout the brain (*1*). In particular, activity shapes the structure of sensory maps (*2*) and individual neurons (*3*) through *N*-methyl-D-aspartate (NMDA) receptor–dependent processes, which suggests that synapse-specific associative changes are involved. Relatively little is known about the role of activity in the development of dendritic morphology. A number of studies have addressed whether long-term potentiation (LTP) produces postsynaptic structural changes. Using electron microscopy (EM) analysis of fixed

Cold Spring Harbor Laboratory, Cold Spring Harbor, NY 11724, USA.

tissue (*4*) and optical imaging of living tissue (*5*), these studies have produced inconsistent results. In the mammalian brain, dendrites develop in a stereotypical sequence: Soon after birth the relatively smooth dendrites of neonates sprout numerous thin filopodia-like protrusions, which are later replaced by dendritic spines as the brain matures (*6*). Studies in developing cultured rat brain slices (*7*) and disassociated cultures (*8–10*) from hippocampal area CA1 show that dendritic protrusions, including filopodia and spines, are structurally dynamic, perhaps powered by actin motility (*10*). Filopodia make synapses that coexist with axodendritic synapses in cultures (*8*, *9*) and in vivo (*11*). These observations have led to the hypothesis that dendritic filopodia are crucial in establishing synaptic connections during development, paving the way for the development of mature spines (*7*, *9*, *11*). Activity-dependent dendritic morphogenesis could therefore underlie Hebbian plasticity during development. We used vital imaging of dendrites in living rat brain slices to directly observe dendritic morphogenesis evoked by synaptic activity.

A small number of CA1 pyramidal neurons in organotypic cultured hippocampal slices (*12*, *13*) were infected with a neurotropic recombinant Sindbis virus (*14*) expressing enhanced green fluorescent protein (EGFP) (*15*) (Fig. 1A). When visualized with a custom-built two-photon laser scanning microscope (TPLSM) (*16*, *17*), infected neurons showed bright homogeneous fluorescence throughout their dendritic and axonal arbors, revealing detailed morphology (Fig. 1, A through C) with numerous dendritic protrusions (the density of the protrusions was 0.52 ± 0.2 μm^{-1}) (*18*). Time-lapse imaging of dendritic segments showed that dendritic morphology is dynamic on time scales of minutes to hours. Protrusions appeared and disappeared or changed shape (Fig. 1D) (*7*).

To examine the effects of synaptic activity on dendritic morphology, a glass electrode (0.4 to 1 megohm) was placed close (~3 to 10 μm) to a target dendrite (Fig. 2A, left). The proximity of the stimulating electrode was absolutely necessary to ensure that the dendrite would receive localized synaptic stimulation (*17*). After the delivery of a tetanic stimulus (two trains of 100 pulses at 100 Hz) in a majority of cases (12 out of 14 experiments) new protrusions appeared (Fig. 2), and the total density of protrusions increased by 19 ± 4% (40 min after tetanus; mean ± SEM, n = 14). Comparison of

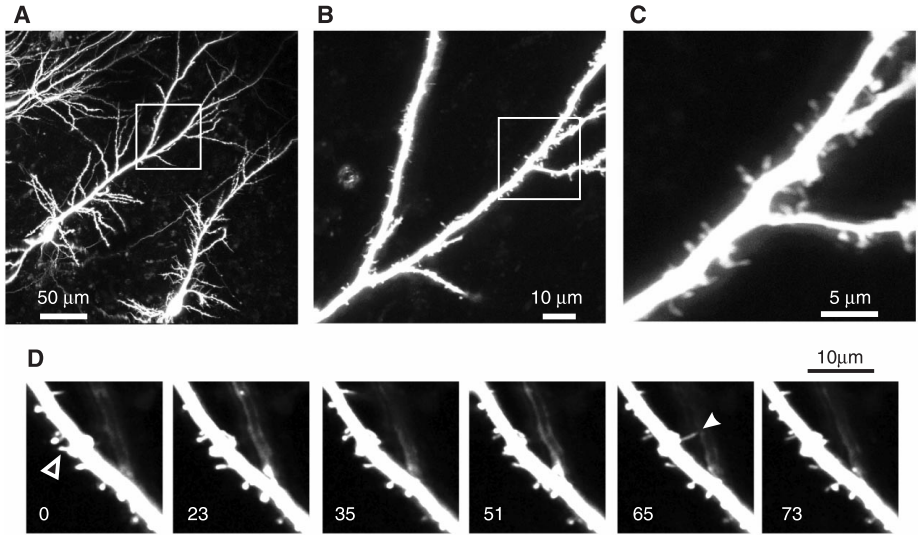

Fig. 1. TPLSM imaging of CA1 pyramidal cell dendrites labeled with EGFP (in a slice 9 days in culture). Images shown are maximum value projections of several sections acquired 0.5 μm apart. (**A**) CA1 region of a hippocampal slice showing several infected neurons, including dendritic arbors and axons. (**B**) Apical dendrite and secondary branches from the boxed region in (A). (**C**) Higher magnification image from the boxed region in (B) showing dendritic protrusions. (**D**) Time-lapse image sequence showing sprouting (solid arrowhead) and retracting (open arrowhead) filopodia (in a slice 9 days in culture; eight sections per image). Time stamps (in minutes) are indicated in the lower left corners.

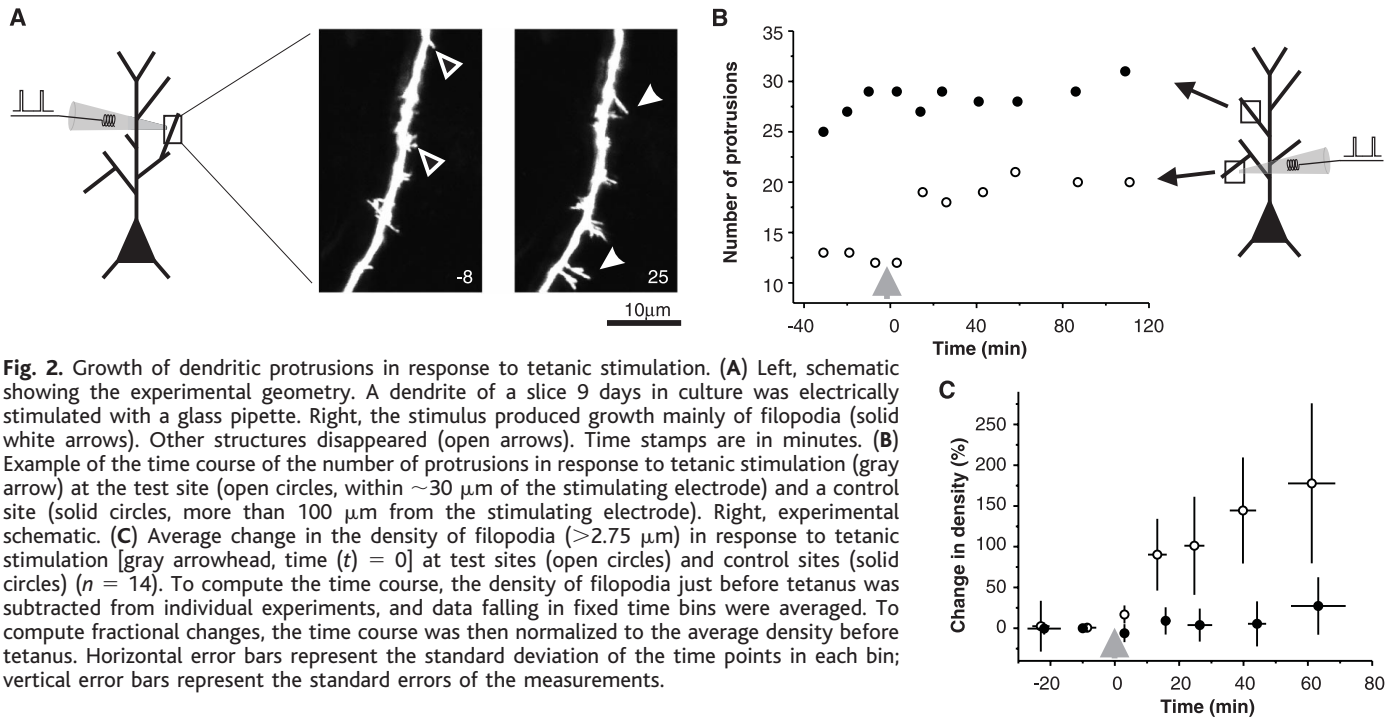

Fig. 2. Growth of dendritic protrusions in response to tetanic stimulation. (**A**) Left, schematic showing the experimental geometry. A dendrite of a slice 9 days in culture was electrically stimulated with a glass pipette. Right, the stimulus produced growth mainly of filopodia (solid white arrows). Other structures disappeared (open arrows). Time stamps are in minutes. (**B**) Example of the time course of the number of protrusions in response to tetanic stimulation (gray arrow) at the test site (open circles, within ~30 μm of the stimulating electrode) and a control site (solid circles, more than 100 μm from the stimulating electrode). Right, experimental schematic. (**C**) Average change in the density of filopodia (>2.75 μm) in response to tetanic stimulation [gray arrowhead, time (t) = 0] at test sites (open circles) and control sites (solid circles) (n = 14). To compute the time course, the density of filopodia just before tetanus was subtracted from individual experiments, and data falling in fixed time bins were averaged. To compute fractional changes, the time course was then normalized to the average density before tetanus. Horizontal error bars represent the standard deviation of the time points in each bin; vertical error bars represent the standard errors of the measurements.

changes in protrusion number after tetanus with changes in the absence of tetanus revealed that tetanus significantly increased the sprouting of new protrusions [$P < 0.005$, Wilcoxon matched-pairs signed-ranks (WMPSR) test] (*19*). Growth began only after a brief delay after tetanus, with no detectable change in dendritic structure at the first time point (3 min; Fig. 2, B and C). Growth was significant 20 min after tetanus and continued for at least another 40 min. The images revealed that the most dramatic feature of tetanus-evoked morphogenesis was an increase in the number of long (>2.75 μm) filopodia-like protrusions (Fig. 2A; length = 4.0 ± 1.5 μm). Before tetanus, filopodia were relatively rare (density = 0.053 ± 0.038 μm^{-1}). Forty minutes after tetanus, their number had increased by 145 ± 65% (mean ± SEM, $n = 14$) (Fig. 2C, open circles). This included de novo genesis of new filopodia >2.75 μm (43%) as well as growth of existing protrusions to lengths exceeding 2.75 μm (57%) (Fig. 2). Because of their pronounced plasticity and their potential role as spine precursors, we focused further analysis on filopodia.

An important property expected for cellular mechanisms underlying circuit formation during development, as well as information

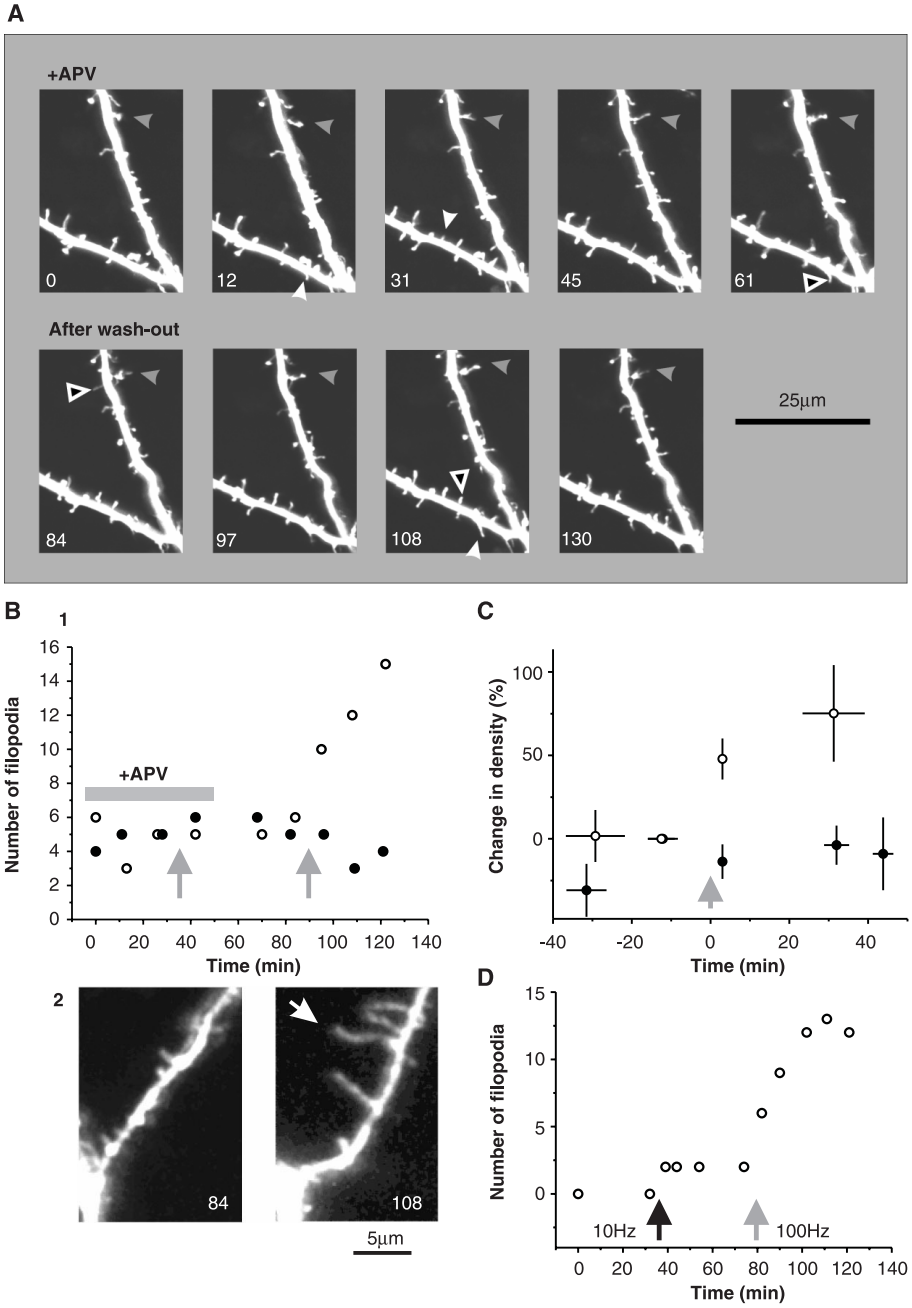

Fig. 3. Dendritic morphogenesis requires synaptic activation of NMDA receptors. (**A**) Time-lapse sequence showing sprouting (white solid arrowheads), retracting (open arrowheads), and changing (grey solid arrowheads) protrusions in the presence (top row) and after washout (bottom row) of APV. Time stamps in (A) and (B) are in minutes. (**B**) 1: Time course of the number of filopodia in response to tetanic stimulation (gray arrows) in the presence of APV (gray bar) and after APV washout (in a slice 8 days in culture). Tetanus in APV produced little change in the number of filopodia. After washout of APV, a subsequent tetanus produced new filopodia. 2: Image of a small side branch before and after tetanus after washout; note the appearance of new filopodia (white arrow). (**C**) Summary data for APV experiments ($n = 8$) expressed as changes in density of filopodia. Error bars, same as in Fig. 2C. (**D**) Example of a time course of the number of filopodia after low-frequency stimulation (10 Hz, black arrow) and a subsequent high-frequency stimulus (100 Hz, gray arrow).

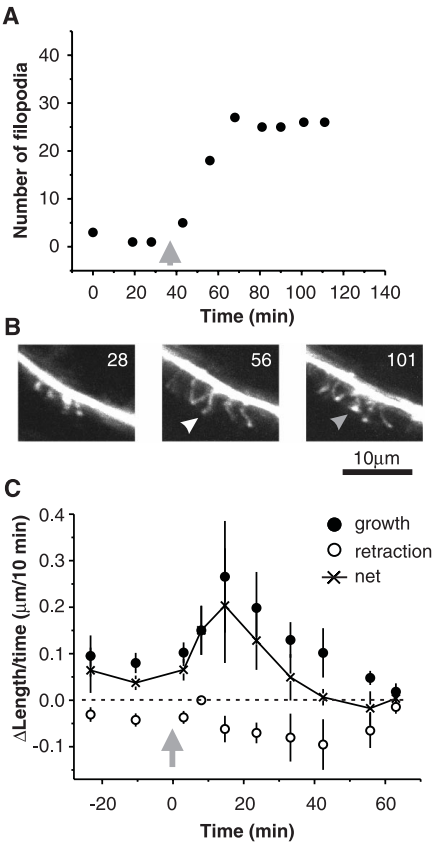

Fig. 4. Time course of the development of dendritic filopodia. (**A**) Example of a time course of the number of filopodia in response to tetanic stimulation at the test site (gray arrow; 100 Hz for 1 s, twice). (**B**) Images corresponding to the time course in (A). Time stamps are in minutes. Tetanic stimulation produced growth of several filopodia (compare 28 min and 56 min, solid white arrowhead) that later developed pronounced bulbous heads (101 min, gray arrowhead). (**C**) Time course of length changes per filopodium between consecutive observations separated by ~10 min (Δlength/time). Growth (crosses, net change; solid circles, change in growing filopodia; open circles, change in retracting filopodia) was delayed by ~5 min and peaked ~15 min after tetanus ($t = 0$, gray arrow) and decayed to baseline within ~40 min.

storage in the adult brain, is that they should be restricted to active synapses (*20*). In our experiments, this would correspond to synapses on dendritic regions close to the stimulating electrode. To test this type of synapse specificity we compared tetanus-induced growth at dendritic sites close to the stimulating electrode (test sites) with dendritic sites at least 100 μm away (control sites). Test sites showed significant growth (Fig. 2C, open circles, $n = 14$), whereas control sites remained unchanged (Fig. 2C, solid circles).

To determine whether growth is stimulated by synaptic transmission rather than by direct depolarization of the postsynaptic membrane by the current from the stimulating electrode, we used D,L(-)-2-amino-5-phosphonopentanoic acid (APV), a specific antagonist for NMDA receptors. Slices were superfused with artificial cerebrospinal fluid (ACSF) containing 100 μM APV while baseline images were collected at test and control sites ($n = 8$). Simple measures of baseline morphological dynamics, such as the rate of formation and retraction of filopodia, were not affected by the presence of APV over the time scale of the experiment (Fig. 3A) (rates of sprouting and retraction were as follows: with APV, $2.5 \pm 2.3\%$ min^{-1}; without APV, $2.3 \pm 2.0\%$ min^{-1}). Delivery of a tetanus in the presence of APV showed that the drug abolished tetanus-evoked morphogenesis, with no significant changes at either the test (Fig. 3, B and C) or control (Fig. 3B) sites. APV was then washed out for >30 min and a second tetanus was delivered, which produced significant growth at the test site (Fig. 3, B and C). The density of filopodia increased significantly when compared to test sites in APV ($P < 0.02$, WMPSR test) and to control sites ($P < 0.02$). Synaptically evoked growth after APV washout was rapid, with significant changes in the number of filopodia occurring only 3 min after tetanus (Fig. 3C). This is in contrast to the experiments in Fig. 2, where a tetanus, without a prior tetanus in APV, produced delayed growth. The reason for this difference is unclear but may reflect some form of priming (*21*) produced by tetanus in APV.

If strong synaptic NMDA receptor activation is required to trigger morphogenesis, then low-frequency stimulation, which leads to much smaller NMDA receptor–mediated postsynaptic currents (*22*), might not produce changes in dendritic morphology. Delivery of 2× 100 stimuli at 10 Hz failed to produce changes in filopodia density that were distinguishable from the baseline ($P = 0.22$, $n = 5$). Subsequent delivery of 100 stimuli at 100 Hz produced a robust increase in the number of filopodia (Fig. 3C).

We examined the morphological fates of filopodia induced by tetanic stimulation. In the absence of additional evoked activity, these structures persisted (Fig. 4, A and B). However, they did not continue to increase in length (Fig. 4C): The net growth decreased to baseline levels ~45 min after tetanus. Furthermore, 27% (19 out of 71) of the new filopodia developed a bulbous head within 1 hour after the stimulus (Fig. 4B), which suggests that filopodia might mature to become spines.

Our results show that synaptic activity can produce rapid growth in postsynaptic dendrites (*23*). Growth was input specific, occurring only close to activated parts of the dendrite, and required synaptic NMDA receptor activation. This activity-induced growth was most prominently expressed as an increase in long, thin, filopodia-like protrusions. Such structures often make synaptic contacts in vivo and in vitro and have been proposed as precursors of mature spines (*7*, *9*, *11*). Consistent with this hypothesis is our observation that new filopodia often develop bulbous heads, a morphological sign of mature spines (*9*, *10*, *24*, *25*) (Fig. 4C). Definite proof that these synaptic activity–induced filopodia make synapses will have to await ultrastructural studies using serial-section EM (*24*) and intracellular measurement of synaptic transmission. If these structures generate synapses, they will have greater likelihood of connecting with presynaptic axons that were active during the synaptic stimulus, providing a mechanism for synaptic plasticity satisfying Hebbian rules. Such a mechanism could play a role in the establishment of functional neural circuits during development and memory storage (*1*, *2*, *20*).

References and Notes

1. T. N. Wiesel, *Nature* **299**, 583 (1982); L. C. Katz and C. J. Shatz, *Science* **274**, 1133 (1996).
2. H. T. Cline, E. A. Debski, M. Constantine-Paton, *Proc. Natl. Acad. Sci. U.S.A.* **84**, 4342 (1987); A. Kleinschmidt, M. F. Bear, W. Singer, *Science* **238**, 355 (1987); K. Fox, N. Daw, H. Sato, D. Czepita, *J. Neurosci.* **12**, 2672 (1992); B. L. Schlaggar, K. Fox, D. D. M. O'Leary, *Nature* **364**, 623 (1993); K. Fox, B. L. Schlagger, S. Glazewski, D. D. O'Leary, *Proc. Natl. Acad. Sci. U.S.A.* **93**, 5584 (1996).
3. H. T. Cline and M. Constantine-Patton, *Neuron* **3**, 413 (1989); R. G. Kalb, *Development* **120**, 3063 (1994); M. W. Vogel and J. Prittie, *J. Neurobiol.* **26**, 537 (1995); A. K. McAllister, L. C. Katz, D. Lo, *Neuron* **17**, 1057 (1996); I. Rajan and H. T. Cline, *J. Neurosci.* **18**, 7836 (1998).
4. E. Fifkova and A. Van Harreveld, *J. Neurocytol.* **6**, 211 (1977); A. Van Harreveld and E. Fifkova, *Exp. Neurol.* **49**, 736 (1975); N. L. Desmond and W. B. Levy, *J. Comp. Neurol.* **253**, 466 (1986); *Synapse* **5**, 139 (1990); K. E. Sorra and K. M. Harris, *J. Neurosci.* **18**, 658 (1998).
5. T. Hosokawa, D. A. Rusakov, T. V. P. Bliss, A. Fine, *J. Neurosci.* **15**, 5560 (1995).
6. H. G. Minkwitz and L. Holz, *J. Hirnforsch.* **16**, 37 (1975); D. Purpura, in *Adv. Neurology*, G. W. Kreutzberg, Ed. (Raven, New York, 1975), vol. 12, pp. 91–116; J. S. Lund, G. R. Boothe, R. D. Lund, *J. Comp. Neurol.* **176**, 149 (1977); M. Miller and A. Peters, *ibid.* **203**, 555 (1981).
7. M. E. Dailey and S. J. Smith, *J. Neurosci.* **16**, 2983 (1996).
8. M. Papa, M. C. Bundman, V. Greenberger, M. Segal, *ibid.* **15**, 1 (1995).
9. N. E. Ziv and S. J. Smith, *Neuron* **17**, 91 (1996).
10. M. Fischer, S. Kaech, D. Knutti, A. Matus, *ibid.* **20**, 847 (1998).
11. Y. Saito *et al.*, *Neurosci. Lett.* **147**, 81 (1992); J. C. Fiala, M. Feinberg, V. Popov, K. M. Harris, *J. Neurosci.* **18**, 8900 (1998).
12. B. H. Gahwiler, M. Capogna, D. Debanne, R. A. McKinney, S. M. Thompson, *Trends Neurosci.* **20**, 471 (1997).
13. Hippocampal slices were prepared from rat pups at postnatal day 7 and were cultured for 7 to 9 days essentially as described (*26*); in some cases ($n = 4$), slices were used after 2 to 5 days in vitro with indistinguishable results. One to two days before use, slices were injected with a solution containing a Sindbis virus carrying the gene for EGFP (*27*). Virus concentrations were used so that approximately one cell was infected per injection site (1 to 10 neurons per slice). Neurons infected with the Sindbis virus remain healthy for at least 3 days, as judged by their resting potential, synaptic transmission, and LTP (*28*). We confined our measurements to tissue derived from young animals because tissue from older animals does not remain viable in culture. Hippocampal circuitry and neuronal morphology continue to develop in cultured slices (*25*).
14. S. Schlesinger, *Trends Biotechnol.* **11**, 18 (1993).
15. M. Chalfie, Y. Tu, G. Euskirchen, W. W. Ward, D. C. Prasher, *Science* **263**, 802 (1994); B. P. Cormack, R. H. Valdivia, S. Falkow, *Gene* **173**, 33 (1996); R. Heim and R. Y. Tsien, *Curr. Biol.* **6**, 178 (1996).
16. W. Denk, J. H. Strickler, W. W. Webb, *Science* **248**, 73 (1990); W. Denk and K. Svoboda, *Neuron* **18**, 351 (1997).
17. Z. F. Mainen *et al.*, *Methods*, in press.
18. TPLSM allowed high-resolution imaging of three-dimensional neuronal structure deep within brain slices (50 to 200 μm). For time-lapse observations, the tissue was placed into a perfusion chamber and superfused continuously (2 ml/min) with ACSF: 119 mM NaCl, 2.5 mM KCl, 4 mM $CaCl_2$, 4 mM $MgCl_2$, 26.2 mM $NaHCO_3$, 1 mM NaH_2PO_4, 11 mM glucose, and 100 μM picrotoxin; then gassed with 95% O_2 and 5% CO_2 at 32° to 33°C. Data acquired at room temperature were indistinguishable but were not used in the analysis. Imaging was performed with a custom-built TPLSM microscope (*17*). The light source was a Ti:Sapphire laser (Mira, Coherent) running at a wavelength of 900 to 910 nm (repetition frequency, 76 MHz; pulse length, 100 fs). The average power delivered to the backfocal plane of the objective (63×, NA 0.9, Zeiss) varied depending on the imaging depth (range, 30 to 200 mW). Fluorescence was detected in whole-field detection mode with a photomultiplier tube (Hamamatsu, R3896). The transillumination light was used to produce a laser scanning DIC image (LSDIC) that had the useful feature that it was perfectly aligned with the fluorescence image. The LSDIC image was used to position the stimulating electrode very close to a selected EGFP-labeled dendrite. Such visual positioning of the stimulation electrode reliably produced synaptic activation of the target dendrite primarily in the vicinity of the electrode, as tested by TPLSM imaging of dendritic calcium generated by synaptic activation (*17*). In contrast, in the same experiments, synaptic stimulation far from the dendrite makes it difficult to find activated synapses. The tetanic stimulus consisted of 2 × 100 Hz (pulse duration, 0.1 ms; pulse amplitude, 10 V), a stimulus that produced LTP in parallel experiments (*28*). The physical configuration of our microscope (fixed stage microscope on an XY translation stage) allowed different dendritic regions on a single neuron to be repeatedly imaged serially by moving the microscope with micrometers. Because of the small depth of focus of the TPLSM microscope, we collected several (10 to 50) sections at 0.5-μm spacing. Laser power was adjusted so that additional power failed to reveal previously undetected protrusions. The quality of labeling and image brightness in EGFP-labeled neurons was comparable to that achieved by labeling with patch electrodes containing 400 μM fluorescein dextran (*29*). Under our experimental conditions, signs of phototoxicity were almost completely absent, even after hours of nearly continuous imaging. In addition, viral labeling avoided injury and washout of intracellular components due to the patch electrode. Dendrites did not change in morphology or morphological dynamics in response to prolonged imaging, which suggests that phototoxicity did not perturb the results.

Variability in Spike Trains During Constant and Dynamic Stimulation

Anne-Kathrin Warzecha* and Martin Egelhaaf

In a recent study, it was concluded that natural time-varying stimuli are represented more reliably in the brain than constant stimuli are. The results presented here disagree with this conclusion, although they were obtained from the same identified neuron (H1) in the fly's visual system. For large parts of the neuron's activity range, the variability of the responses was very similar for constant and time-varying stimuli and was considerably smaller than that in many visual interneurons of vertebrates.

The reliability of behavioral responses to external events is limited by neuronal variability. Neuronal variability is commonly quantified by the variance in the number of spikes in response to repetitive presentations of identical stimuli. Variances across trials have often been found to be on the order of the mean spike count (*1–7*). Recently, the idea has been put forward (*1, 8*) that neuronal variability is only as large as the mean spike count if the responses are elicited by more or less constant stimuli. In contrast, it was concluded that more naturalistic dynamic stimuli elicit spike trains that are much more reproducible and thus have considerably smaller variances. Although it is thought that the reliability of neural coding is especially adapted to stimuli encountered by an animal in its natural behavioral context (*1*), our study does not support this hypothesis. Our experimental analysis was carried out on an identified neuron in the fly visual system, the H1 neuron, which has often been used to analyze the reliability of processing visual motion (*1, 9–16*).

The H1 neuron responds selectively to the direction of motion in large parts of the visual field by integrating the output signals of many local motion-sensitive elements. It increases its spike rate above the resting level during back-to-front motion (preferred direction) and decreases the spike rate during motion in the opposite direction (null direction). Because the spontaneous activity of the H1 cell is low, it usually stops firing when the pattern moves in the null direction (*9, 16*). Examples of how visual motion is represented by the H1 neuron are shown in Fig. 1 (*17*). The fly was stimulated by motion with different dynamical properties, that is, either by a pattern moving at a constant velocity or by random velocity fluctuations (*18*). At the onset of constant-velocity stimulation, the spike activity of the H1 neuron increased and, after a transient phase, reached a more or less constant level. During dynamic stimulation, the spike activity fluctuated strongly, following (to some extent) the time course of pattern velocity (Fig. 1D) (*11, 15, 19*). The timing of spikes was not entirely determined by the motion stimulus. It was also controlled by stimulus-independent sources, which becomes obvious when comparing individual response traces that were elicited by identical motion stimuli (Fig. 1, E and F). The variability was quantified by determining the variance in the number of spikes within a given time window in relation to the stimulus onset. For constant- and dynamic-velocity stimulation, the variance across trials was determined for a range of window sizes and was plotted as a function of the mean spike count. Because the stimulus-induced response to constant-velocity motion did not modulate much over time, only a small range of activities was elicited by a given stimulus (Fig. 1C). Therefore, the stimulus strength was altered by changing the vertical extent of the pattern. In contrast, during dynamic stimulation, the spike frequency was strongly modulated over the entire activity range of the H1 neuron (Fig. 1D). The variances obtained within 10-ms time windows were very similar for the two different stimulus dynamics. For constant as well as for dynamic stimulation, the plot of variance versus mean spike count was scalloped (Fig. 2). The variance was very small when the mean spike count was close to an integer number, and the variance was largest for intermediate spike counts. The scalloped distribution of data points is due to the discreteness of spikes [for a detailed explanation, see (*1*)]. The scallops closely followed the minimal variance that could be obtained in a spiking neuron (dotted lines in Fig. 2, A and B). The qualitative features of the single-cell example (Fig. 2, A and B) were corroborated by the mean variance averaged over several cells (Fig. 2, C and D). Hence, the variability of responses of the H1 cell was not influenced by the stimulus dynamics when it was evaluated within

Lehrstuhl für Neurobiologie, Fakultät für Biologie, Universität Bielefeld, Postfach 10 01 31, D-33501 Bielefeld, Germany.

*To whom correspondence should be addressed. E-mail: ak.warzecha@biologie.uni-bielefeld.de

19. Typically, pairs of stacks of images of secondary and tertiary dendritic branches (test and control sites) were collected at ~15-min intervals. Images were stored digitally and analyzed offline essentially unprocessed. The numbers and lengths of protrusions (lower limit, 0.54 μm) in a field of view (45 μm by 45 μm) containing 69 ± 22 μm of dendritic length were measured, keeping track of the fates of individual structures in optical sections. The limited *z*-resolution of our microscope (~1.5 μm) did not allow us to reliably detect and analyze protrusions that did not project laterally from the dendritic shaft, resulting in an underestimate of the densities of protrusions. Measurements were done in two-dimensional projections, resulting in an underestimate of the lengths of protrusions. To calculate the error resulting from projections, let r be the dendritic radius and l the length of spiny protrusions. Then the length of the projection of the protrusion—the measured length l'—is given by $l' = [(l + r)\cos\theta - r]$, where θ is the angle with respect to the horizontal. Assuming that spines are distributed isotropically, we can compute the average length as

$$\langle l' \rangle = (1/\theta_0) \int_0^{\theta_0} l' d\theta$$

where θ_0 is the largest angle for which protrusions are measured ($<\pi/4$). To estimate an upper bound for the error, we assume $l' = 2.75$ μm and $r = 0.5$ μm, and solve for l. This calculation suggests that we might underestimate the true length of protrusions by up to 13%. Only one set of experiments was performed per neuron (n refers to the number of neurons). Changes in the number of protrusions after tetanus were distributed in a non-Gaussian manner. In particular, our data probably included some experiments where the stimulating electrode failed to evoke synaptic responses on the target dendrite. We therefore used nonparametric statistics to test for differences in changes in morphometric distributions (*30*). Significance levels were computed with the WMPSR test and in all cases agreed with the highly restrictive sign test. Measurements are given as mean ± SD unless otherwise indicated.

20. T. V. P. Bliss and G. L. Collingridge, *Nature* **361**, 31 (1993); A. Kirkwood, H.-K. Lee, M. F. Bear, *ibid.* **375**, 328 (1995); M. C. Crair and R. C. Malenka, *ibid.*, p. 325; K. D. Miller, *Neural Comput.* **10**, 529 (1998).
21. Z. A. Bortolotto, Z. I. Bashir, C. H. Davies, G. L. Collingridge, *Nature* **368**, 740 (1994).
22. G. L. Collingridge, C. E. Herron, R. A. Lester, *J. Physiol.* **399**, 301 (1988).
23. These findings differ from previous studies designed to search for structural correlates of LTP (*4, 5*). One reason could be that we used developing tissue; another reason could be the fact that we limited our structural analysis to regions of the dendrites that contained most of the activated synapses, thus improving the signal-to-noise ratio; a third factor could be that filopodia may be difficult to detect with EM.
24. K. M. Harris and J. K. Stevens, *J. Neurosci.* **9**, 2982 (1989).
25. C. Collin, K. Miyaguchi, M. Segal, *J. Neurophysiol.* **77**, 1614 (1997).
26. L. Stoppini, P. A. Buchs, D. A. Muller, *J. Neurosci. Methods* **37**, 173 (1991).
27. R. Malinow *et al.*, in *Imaging Living Cells*, R. Yuste, F. Lanni, A. Konnerth, Eds. (Cold Spring Harbor Laboratory Press, Cold Spring Harbor, NY, in press).
28. S. H. Shi *et al.*, data not shown.
29. K. Svoboda, D. W. Tank, W. Denk, *Science* **272**, 716 (1996).
30. S. Siegel, *Nonparametric Statistics* (McGraw-Hill, New York, ed. 1, 1956).
31. Supported by NIH (M.M.-S., R.M., and K.S.), the Mathers Foundation (R.M.), the Human Frontiers Science Program, and the Pew and Whitaker Foundations (K.S.). We thank B. Lendvai and E. Nimchinsky for helpful suggestions and B. Burbach, N. Dawkins, and S. Shi for technical assistance.

11 September 1998; accepted 8 February 1999